Supplementary Materials and Methods

Immunohistochemical Analysis

Immunohistochemical analysis of frozen and paraffin sections was performed as previously described.[1] Primary antibodies were the following: rabbit anti-amylase (1:1000; Sigma, St. Louis, MO); goat anti-amylase (1:100; Santa Cruz Biotechnology, Santa Cruz, CA); sheep anti-amylase (1:400; Abcam, Cambridge, MA); rabbit anti-Sox9 (1:250; Chemicon, Billercia, MA); rabbit anti-Mist1 (1:500; provided by S. Konieczny); rabbit anti-mucin (1:50; Santa Cruz Biotechnology, Santa Cruz, CA); goat anti-mucin (1:25; Santa Cruz Biotechnology); rabbit anti-mucin (1:200; Abcam); hamster anti-mucin (1:500; Thermo Scientific, Waltham, MA); mouse anti-acetylated β-tubulin (1:4,000; Sigma); rabbit anti-elastase (1:2000; Abcam); goat anti-osteopontin (1:25; R&D Systems, Minneapolis, MN); rabbit anti-synaptophysin (1:1000; Invitrogen, Grand Island, NY); chicken anti–β-galactosidase (1:2,000; Abcam); rabbit anti-Pdx1 (1:1000; provided by C. Wright); rabbit anti-Prox1 (1:1000; AngioBio, Del Mar, CA); rat anti-uvomorulin/E-cadherin (1:10,000; Sigma); rabbit anti-CD3 (1:250; Abcam); rat anti-mouse CD45R (1:500; Santa Cruz Biotechnology); rabbit anti-Mac2 (1:250; Santa Cruz Biotechnology); rat anti-F4/80 (1:3000; Caltag, Grand Island, NY); rat anti-CD65 (1.100; ABD Serotec, Raleigh, NC); rat anti-mouse neutrophils (1:2500; Caltag); rabbit anti–claudin-2 (1:400; Spring Bioscience, Pleasanton, CA); rabbit anti–claudin-2 (1:500; Abcam); rabbit anti–claudin-1 (1:100; Invitrogen); rabbit anti–claudin-3 (1:250; Invitrogen); rabbit anti–claudin-7 (1:250; Spring Bioscience); rat anti-ZO1 (1:500; Millipore, Billercia, MA); guinea pig anti-ngn3 (1:2,000; provided by M. German); rat anti-Ki67 peptide (1:1,000; Neomarkers, Waltham, MA); and mouse anti–MAP kinase peptide, diphosphorylated ERK-1/2 (1:1,000; Sigma). The secondary antibodies (diluted 1:200) were Cy3-conjugated donkey anti-guinea pig immunoglobulin (Ig) G (Jackson ImmunoResearch Laboratories, Inc, West Grove, PA); Cy3-conjugated donkey anti-rabbit IgG (Jackson ImmunoResearch Laboratories, Inc); Cy3-conjugated donkey anti-goat IgG (Jackson ImmunoResearch Laboratories, Inc); Cy3-conjugated goat anti-chicken IgG (Rockland, Gilbertville, PA); Alexa 488–conjugated donkey anti-rabbit IgG (Molecular Probes, Grand Island, NY); Alexa 488–conjugated donkey anti-rat IgG (Molecular Probes); Alexa 488–conjugated goat anti–guinea pig IgG (Molecular Probes); Alexa 488–conjugated donkey anti-goat IgG (Molecular Probes); Alexa 488–conjugated donkey anti-mouse IgG (Molecular Probes); Alexa 488–conjugated goat anti-chicken IgG (Molecular Probes); AMCA-conjugated donkey anti-rabbit (Jackson ImmunoResearch Laboratories, Inc); AMCA-conjugated goat anti-hamster (Jackson ImmunoResearch Laboratories, Inc); and AMCA-conjugated donkey anti-sheep (Jackson ImmunoResearch Laboratories, Inc). Biotinylated donkey IgG antibodies (anti-rabbit, anti-guinea pig, anti-mouse, or anti-goat; Jackson ImmunoResearch Laboratories, Inc) were detected by using the Vectastain Elite ABC kit (Vector Laboratories, Burlingame, CA). 4′,6-Diamidino-2-phenylindole (DAPI) (Vectashield; Vector Laboratories) was used for nuclear staining. For DBA staining, we used fluorescein-conjugated Dolichos biflorus agglutinin (1:500; Vector Laboratories). Images were obtained either with a Zeiss (Oberkochen, Germany) Axioskop 2 microscope or with a confocal/multiphoton laser-scanning Zeiss LSM 510 META microscope.

Statistical Analyses

Statistical significance was determined using Student *t* test ($P < .05$ indicates statistically significant differences).

Histology

H&E, alcian blue (Sigma), diastase/periodic acid–Schiff (Sigma), Masson's trichrome (Poly Scientific, Bay Shore, NY), and oil red O solution (Sigma) staining was performed per the manufacturer's directions.

TUNEL Assay

Apoptosis was detected using the ApopTag Fluorescein In Situ Apoptosis Detection Kit (Chemicon) or Klenow-Frag-EL kit (Oncogene Research Products, La Jolla, CA) per the manufacturer's directions.

Electron Microscopy

P7 control and *Prox1*$^{\Delta Panc}$ pancreatic tissues were fixed in 4% glutaraldehyde in 0.1 mol/L sodium cacodylate and processed using standard laboratory techniques.

Western Blot

Pancreata were isolated from several postnatal stages (P10, P15, and P22), flash frozen, and powered in liquid nitrogen. Samples were sonicated for 30 seconds in cold lysis buffer (50 mmol/L Tris-HCl, pH 7.2, 10 mmol/L dithiothreitol, 1% Nonidet P-40, 1 mmol/L $CaCl_2$, 5 mmol/L $MgCl_2$, and Complete Protease Inhibitor Cocktail tablets [Roche, Indianapolis, IN]). Lysates were microcentrifuged at 4°C for 5 minutes. A total of 15 μg of total protein was loaded per lane. Sodium dodecyl sulfate/polyacrylamide gel electrophoresis, protein transfer, and Western blotting were performed using standard laboratory techniques. Primary antibodies were the following: rabbit anti–carboxypeptidase A (1:4000; AbSerotec, Raleigh, NC), rabbit anti-amylase (1:1000; Santa Cruz Biotechnology), and mouse anti–β-actin (1:5000; Sigma). The following secondary antibodies were used: goat anti-rabbit horseradish peroxidase conjugated (1:2000; Pierce, Waltham, MA) and goat anti-mouse horseradish peroxidase conjugated (1:4000; Pierce). SuperSignal West Pico chemiluminescent substrate (Thermo Scientific) was used.

In Situ Hybridization

Digoxigenin-labeled antisense *neurogenin* (*Ngn3*) messenger RNA probes were transcribed in vitro using plasmids provided by D. Anderson. In situ hybridization was performed as described.[2]

Quantitative Real-Time PCR

Total RNA was extracted from at least 3 individual control or $Prox1^{\Delta Panc}$ pancreata using TRIzol (Invitrogen). Complementary DNA was generated using either SuperScript III reverse transcriptase (Invitrogen) or TaqMan Reverse Transcription Reagent (Applied Biosystems, Grand Island, NY) following the manufacturer's recommendations. 18S ribosomal RNA (TaqMan probe, Grand Island, NY) or β-actin (SYBR Green reagent; Applied Biosystems) were used as internal controls and for normalization. The expression of all other genes was determined using SYBR Green reagent and gene-specific primers (Supplementary Table 1). $2^{\Delta\Delta Ct}$ method was used for quantification of each gene of interest.

Supplementary References

1. Westmoreland JJ, Wang Q, Bouzaffour M, et al. Pdk1 activity controls proliferation, survival, and growth of developing pancreatic cells. Dev Biol 2009;334:285–298.
2. Wang J, Kilic G, Aydin M, et al. Prox1 activity controls pancreas morphogenesis and participates in the production of "secondary transition" pancreatic endocrine cells. Dev Biol 2005;286:182–194.

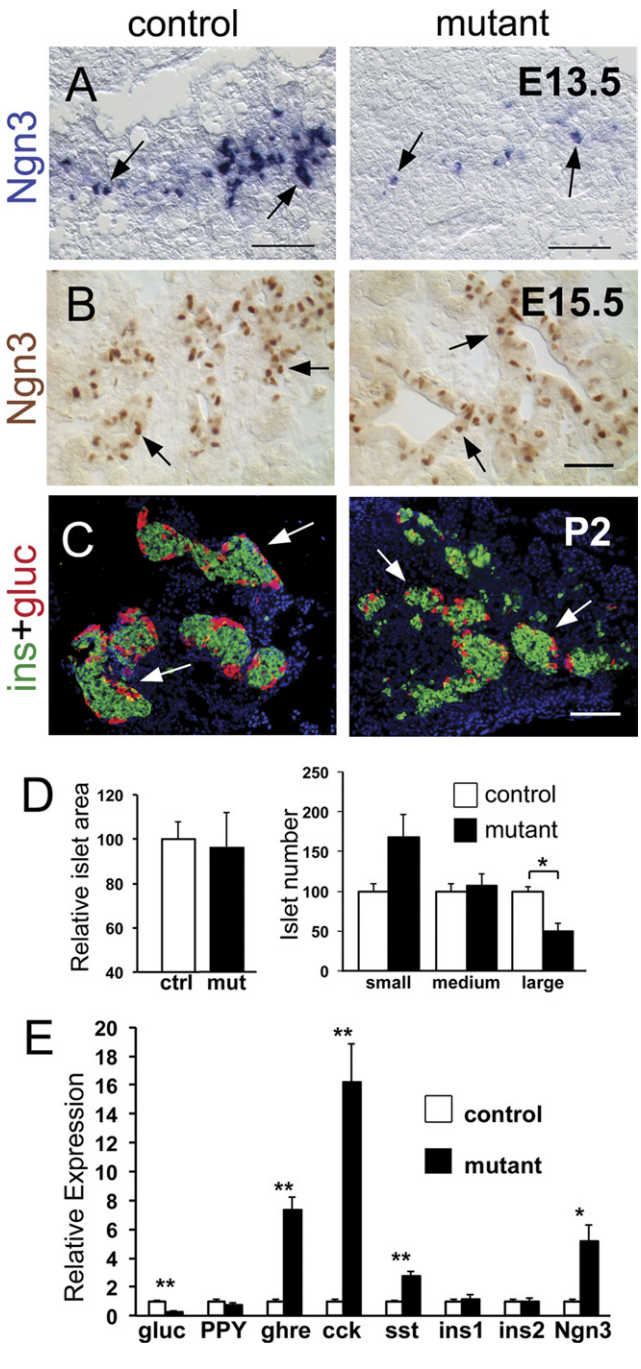

Supplementary Figure 1. Loss of Prox1 function affects the timing of islet cell genesis and causes imbalanced production of some islet hormones. Endocrine precursors (Ngn3-positive cells, *arrows*) are substantially reduced in *Prox1*$^{\Delta Panc}$ pancreata at 13.5 (*A*), but their numbers begin to restore after E15.5 (*B*, *arrows* indicate Ngn3-expressing cells) in these mutant tissues. (*C*) Numerous islets (*arrows*) are observed in the pancreas of control (*left*) or *Prox1*$^{\Delta Panc}$ mice (*right*) shortly after birth. (*D*) Morphometric analysis results show no differences in relative islet mass (synaptophysin-positive area), but significantly less large islets, in *Prox1*$^{\Delta Panc}$ versus control pancreata at P2 (n = 3; islet size was determined using ImageJ 1.37v software [National Institutes of Health] and arbitrarily selected as follows: large islets >800 pixels, medium islets 501–799 pixels, small islets <500 pixels). (*E*) qRT-PCR (n = 4–5) results show increased expression of *ghrelin*, *cck*, and *sst*; decreased expression of *glucagon*; and no changes in *PPY*, *insulin1*, and *insulin2* transcript expression in pancreata lacking Prox1 compared with control tissues at P5. The increased expression of *Ngn3* in *Prox1*$^{\Delta Panc}$ pancreata suggests an extension of the islet cell genesis period in these mutant tissues. Ngn3 expression was detected with an antisense *Ngn3* probe in *panel A* and with anti-Ngn3 antibodies in *panel B*. *Scale bars* = (*A* and *B*) 50 μm and (*C*) 100 μm. *$P < .05$, **$P < .01$.

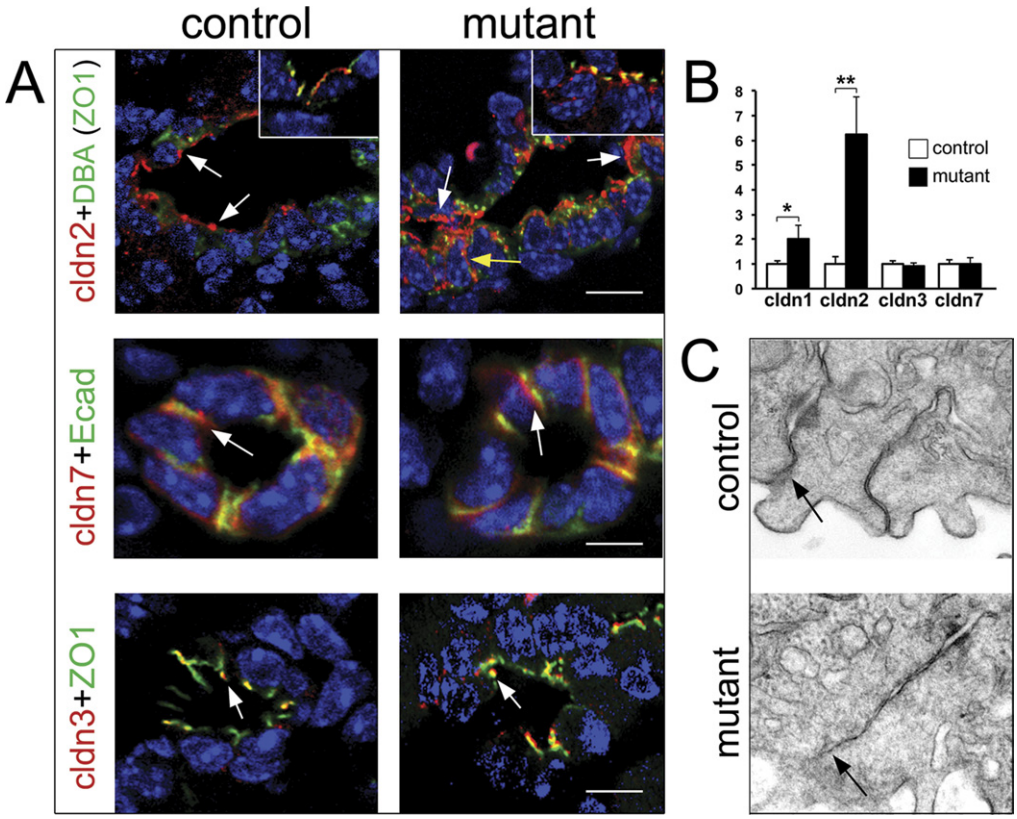

Supplementary Figure 2. Loss of *Prox1* selectively affects the expression of claudin proteins but not tight junction formation in pancreatic duct epithelia. (*A*, *top, left*) Claudin-2 proteins specifically distribute on the apical side of the control pancreatic duct epithelium (stained with fluorescence-labeled Dolichos biflorus agglutinin [DBA]), where they colocalize with the tight junction protein ZO-1 (*inset*). (*A*, *top*, *right*) Claudin-2 proteins are noticeably more abundant in the *Prox1*$^{\Delta Panc}$ pancreatic duct epithelium, and they distribute on both the apical and lateral membranes as well as in the tight junctions (*inset*). (*A*, *middle*) Claudin-7 proteins distribute on both the apical and lateral membranes (*arrows*) of the control pancreatic duct epithelium (*left*), and this pattern remains unaltered in *Prox1*$^{\Delta Panc}$ duct epithelia (*right*). (*A*, *bottom*) Claudin-3 proteins have similar colocalization with ZO-1 (*arrows*) in both control and *Prox1*$^{\Delta Panc}$ duct epithelia. (*B*) qRT-PCR results show significantly increased expression of *claudin1* and *claudin2* transcripts, but normal expression of *claudin3* and *claudin7* transcripts in *Prox1*$^{\Delta Panc}$ pancreata compared with control pancreata at P5 (n = 4–5). (*C*) TEM images show comparable tight junctions in *Prox1*$^{\Delta Panc}$ and control pancreatic ducts at P7 (original magnification ×60,000). *Panel A* shows confocal images of pancreata dissected at P5. *Scale bars* = (*A*, *top*, *bottom*) 10 μm and (*A*, *middle*) 7 μm. *$P < .05$, **$P < .01$.

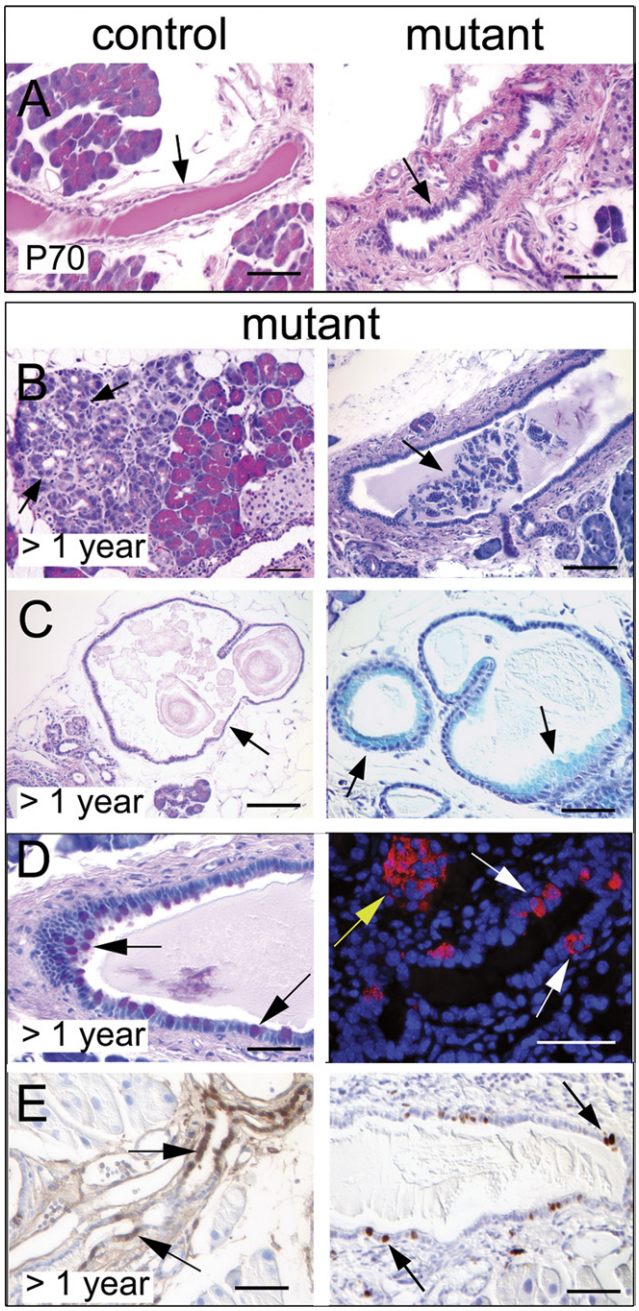

Supplementary Figure 3. *Prox1*$^{\Delta Panc}$ adult pancreata have ductal features indicative of tissue damage. (*A*) Different from control ducts, the pancreatic duct epithelium of *Prox1*$^{\Delta Panc}$ adult (P70) mice appears rugged and hyperplastic (*arrows*). *Prox1*$^{\Delta Panc}$ adult pancreata also have ductal features indicative of tissue damage and possible activation of regenerative responses, including acinar-to-ductal metaplasias (*B*, *left*, *arrows*; notice the relatively normal adjacent acinar tissue); debris accumulation in the lumen of large ducts (*B*, *right*, *arrows*); cysts (*C*, *left*, *arrow*) and structures with abundant cytoplasm (*C*, *right*, *arrows* [alcian blue positive]); presence of goblet cells (*D*, *left*, *arrows* [periodic acid–Schiff positive]) or insulin-expressing cells within the ductal epithelium (*D*, *right*, *white arrows*; *yellow arrow* is an islet); and cells with active mitogen-activated protein signaling (*E*, *left*, *arrows* [p-ERK1/2^{+}]) or undergoing proliferation (*E*, *right*, *arrows* [Ki67^{+}]). *Scale bars* = (*A*, *C–E*) 50 μm and (*B*) 100 μm.

Supplementary Table 1. Primers for Real-Time PCR

	Forward	Reverse
β-actin	CTAAGGCCAACCGTGAAAAG	ACCAGAGGCATACAGGGACA
Ngn3	GAACTAGGATGGCGCCTCAT	CGGGAAAAGGTTGTTGTGTCTCT
Ptf1a	GGGACGAGCAAGCAGAAGTA	CGCGGTAGCAGTATTCGTG
Claudin1	CTTGACCCCCATCAATGC	CACCTCCCAGAAGGCAGA
Claudin2	TGAACACGGACCACTGAAAG	TTAGCAGGAAGCTGGGTCAG
Claudin3	TGGGAGCTGGGTTGTACG	CAGGAGCAACACAGCAAGG
Claudin7	GACGCCCATGAACGTTAAGTA	CCTGGACAGGAGCAAGAGAG
Prox1	CGCAGAAGGACTCTCTTTGTC	GATTGGGTGATAGCCCTTCAT
Amylase	GTGGAATGGCGAGAAGATGT	CTCTGTCAGAAGGCACCAAA
Mist1	GGCTAAAGCTACGTGTCCTTG	GGTGAGGCCCTTCCAACT
Insulin 1	CAGAGAGGAGGTACTTTGGACTATAAA	GCCATGTTGAAACAATGACCT
Insulin 2	GAAGTGGAGGACCCACAAGTG	CTGAAGGTCCCCGGGGCT
Ghrelin	CCAGAGGACAGAGGACAAGC	CATCGAAGGGAGCATTGAAC
Somatostatin	CCCAGACTCCGTCAGTTTCT	GGGCATCATTCTCTGTCTGG
Pancreatic polypeptide	TCACTAGCTCAGCACACAGGA	CCACCCAAGTGGATACGAGA
Glucagon	GCCCTTCAAGACACAGAGGA	CCTCATGCGCTTCTGTCTG
Cholecystokinin	AGCGCGATACATCCAGCAG	ACGATGGGTATTCGTAGTCCTC